



**HAL**  
open science

## Self potential signals preceding variations of fumarole activity at Merapi volcano, Central Java.

Svetlana Byrdina, C. Rücker, M. Zimmer, S. Friedel, U. Serfling

► **To cite this version:**

Svetlana Byrdina, C. Rücker, M. Zimmer, S. Friedel, U. Serfling. Self potential signals preceding variations of fumarole activity at Merapi volcano, Central Java.. *Journal of Volcanology and Geothermal Research*, 2012, 215-216, pp.40-47. 10.1016/j.jvolgeores.2011.12.002 . insu-00786520

**HAL Id: insu-00786520**

**<https://insu.hal.science/insu-00786520v1>**

Submitted on 8 Feb 2013

**HAL** is a multi-disciplinary open access archive for the deposit and dissemination of scientific research documents, whether they are published or not. The documents may come from teaching and research institutions in France or abroad, or from public or private research centers.

L'archive ouverte pluridisciplinaire **HAL**, est destinée au dépôt et à la diffusion de documents scientifiques de niveau recherche, publiés ou non, émanant des établissements d'enseignement et de recherche français ou étrangers, des laboratoires publics ou privés.

# Self potential signals preceding variations of fumarole activity at Merapi volcano, Central Java.

S. Byrdina<sup>a,\*</sup>, C. Rücker<sup>b</sup>, M. Zimmer<sup>c</sup>, S. Friedel<sup>d</sup>, U. Serfling<sup>e</sup>

<sup>a</sup>*ISTerre, Université de Savoie, Equipe Géophysique des Volcans, IRD R219, CNRS, UMR 5559, F-73376 Bourget du Lac, France*

<sup>b</sup>*Technische Universität Berlin, Institut für Angewandte Geowissenschaften, Ackerstr. 76, D-13355 Berlin*

<sup>c</sup>*Helmholtz-Centre Potsdam GFZ German Research Center for Geosciences, Telegrafenberg, 14473 Potsdam, Germany*

<sup>d</sup>*COMSOL Multiphysics GmbH, Technoparkstr. 1, 8005 Zürich, Switzerland*

<sup>e</sup>*GGL Geophysik und Geotechnik Leipzig GmbH, Bautzner Str. 67, 04347 Leipzig*

---

## Abstract

This paper analyzes simultaneous self-potential and gas temperature variations recorded at Merapi volcano in spring 2001, the dry season shortly after the volcanic crisis 2001. Temporal variations of fumarole gas temperature show characteristic quasi periodic signals at scales 1-8 hours and amplitudes up to ten degrees. We propose a simple graphical technique combining a wavelet scalogram and a cross-correlation analysis to demonstrate that the variations of gas temperature are systematically preceded by self-potential variations at the same scales. The influence of meteorological variations on these correlated signals can be ruled out. Rather, we suggest them to be related to the magma degassing in the upper conduits of the volcano. We discuss a semi-qualitative model to explain this correlation and the observed phase shift of about two hours.

*Keywords:* self-potential monitoring, hydrothermal system, gas monitoring, Merapi

---

## 1. Introduction

Merapi is one of the most active volcanoes in Indonesia, located on the Java Arc (Figure 1), where the Indo-Australian Plate is subducted beneath the Java Trench. Its characteristic activity consists of sequences of growth and gravitational collapse of a viscous andesitic dome (Voight et al., 2000) producing pyroclastic flows. In addition to this regular activity, Voight et al. (2000) describe

---

\*Corresponding author

*Email addresses:* svetlana.byrdina@univ-savoie.fr (S. Byrdina), carsten.ruecker@tu-berlin.de (C. Rücker), martin.zimmer@gfz-potsdam.de (M. Zimmer), sven.friedel@comsol.com (S. Friedel), serfling@ggl-gmbh.de (U. Serfling)

6 several major eruptions with  $VEI > 2$  since 1768, like the explosion in 1822 which created a circular  
7 crater with 600 m diameter; the 1872 explosion completely destroyed the dome and created an  
8 oval crater 500 m deep; the eruption in 1930 with dome destruction and pyroclastic flows traveling  
9 up to 12 km. The time interval studied in the current paper was preceded by few months by  
10 a partial dome collapse, occurred in early 2001. This minor event was typical for the activity  
11 of Merapi volcano in twentieth century. Two months before the first dome collapse an increase  
12 in frequency of volcano-tectonic and multi-phase earthquakes was observed, thereafter numerous  
13 pyroclastic flows were encountered which accompanied the growth of the new lava dome. The new  
14 dome reached a total volume of about  $1.4 \times 10^6 \text{ m}^3$  before it partially collapsed in two stages on  
15 January 28 and February 10.

16 The latest to date explosive crisis which happened in October-November 2010 was probably the  
17 most violent eruption since 1872. During this eruption with  $VEI \approx 4$ , a new summit crater with a  
18 diameter of 400 m was created, released  $\approx 0.44 \text{ Tg}$  of  $\text{SO}_2$ , caused evacuation in a 20 km radius from  
19 the volcano and more than 350 fatalities (Surono et al., 2011). This dangerous eruption behavior  
20 with possible influence of external factors like rainfall or tectonic activity (e.g. Voight et al., 2000;  
21 Friedel et al., 2004; Harris and Ripepe, 2007; Surono et al., 2011) motivates further studies aimed  
22 to improve multi-parameter monitoring techniques.

23 Traditional Merapi monitoring techniques include seismology, deformation, in-situ sampling  
24 of gas emissions, and petrology (e.g. Surono et al., 2011, and references there) by the Indonesian  
25 Center of Volcanology and Geological Hazard Mitigation and its observatory and technology center  
26 in Yogyakarta, BPPTK. Continuous monitoring of geochemical parameters at the summit of Merapi  
27 was conducted during few weeks in 1998 and in 2000, when an automatic gas monitoring unit  
28 comprising gas chromatograph, an alpha scintillometer and temperature sensor was installed at  
29 Solfatara field Woro (Zimmer and Erzinger, 2003). The authors observed cyclic variations in the  
30 chemical composition of the gas associated with variations of its temperature. The gas temperature  
31 was found to increase when the concentration of the  $\text{CO}_2$  increased and the concentration of  $\text{H}_2\text{O}$   
32 decreased (Figure 2).

33 The self-potential method is often used to characterize the extension of hydrothermal system,  
34 complimentary to geochemical data (Lénat et al., 2000; Finizola et al., 2004; Revil et al., 2008;  
35 Byrdina et al., 2009). The major contributions of self-potential are created by the flow of the

36 pore water dragging an excess of electrical charges existing in the vicinity of the mineral/water  
37 interface, the so-called streaming potential (e.g. Nourbehecht, 1963; Ishido and Mizutani, 1981;  
38 Revil et al., 1999, 2003; Crespy et al., 2008). At Merapi volcano, a continuous monitoring of  
39 self-potential and ground temperatures was conducted from August, 2000 to July, 2001, in order to  
40 retrieve information on subsurface water flow variations related to the volcanic activity (Friedel  
41 et al., 2004). A clear correlation between self-potential, and seismic signals in ultra low frequency  
42 band was observed before the volcanic crisis in the early 2001, mostly during the rain season in  
43 November 2000 - January 2001 (Byrdina et al., 2003). Because of the strong influence of rainfall on  
44 self-potential and temperature, only repetitive or high-amplitude signals could be studied during  
45 the rain season. The present work deals with analysis of gas flow characteristics in Woro fumarole  
46 in dry season and during the period of relative quiescence following the 2001 volcanic crisis. The  
47 aim of the present work is to detect the common gas temperature and the self-potential signals  
48 reflecting the variations in magmatic degassing during an inter-eruptive period.

## 49 **2. Experiment and Instruments**

50 A continuous monitoring station for electrical field and ground temperatures was installed in  
51 August 2000, in 200 m distance from the dome and several meters away from the fumarolic vents  
52 of Woro (Figure 1 b). The station included three electrode pairs, two in North-South direction  
53 with lengths of 50 and 75 m and one in East-West direction of 50 m length. We called them in the  
54 following the SP dipoles  $U_{21}$ ,  $U_{43}$ , and  $U_{65}$ . Two electrodes,  $E_2$  and  $E_5$ , were placed in a direct  
55 vicinity of fumarole vents,  $E_5$  was only few meters away from the fumarole temperature sensor  
56 GC. We used non-polarizable Ag/AgCl electrodes designed by the Geophysical Instrument Pool  
57 Potsdam. Voltage differences were sampled at 20 sps with a resolution of  $0.2 \mu\text{V}$ . Each electrode was  
58 equipped with a PT1000 temperature sensor at the depth of installation 0.7-0.8 m. The temperature  
59 data were sampled at 4 sps with a resolution of  $0.1^\circ\text{C}$  using a Guralp CMG 24 digitizer with GPS  
60 clock synchronization. We refer to Friedel et al. (2004) for a more detailed description of the  
61 setup. In the following, analogous to the notation of Friedel et al. (2004), the self-potential data  
62 are referred to as  $U_{21} = U_2 - U_1$ , the potential difference measured between the electrodes  $E_2$  and  
63  $E_1$  etc. Similarly, the difference of the ground temperature at the electrode positions (called in  
64 the following electrode temperature difference)  $T_{21} = T_2 - T_1$  etc. Ground temperatures varied

65 between 40 and 70 °C except for sensor  $T_4$  whose maximal temperature reached 100 °C. In order  
 66 to obtain the same sampling as for gas temperature, all data were down-sampled to 1 sample per  
 67 minute using median filtering. The median was preferred to simple moving averages or low-pass  
 68 filters in the frequency domain because of its robustness against outliers.

69 The fumarole gas temperature sensor, a Ni-Cr/Ni thermocouple at 30 cm depth, replaced a gas  
 70 chromatograph installed in 1998 at a location indicated as GC in Figure 1 c (for more details see  
 71 Zimmer and Erzinger, 2003). During the main dome collapse of February 10, 2001, the station was  
 72 partially destroyed and was be reactivated 2 months later starting on April 6, 2001.

### 73 3. Data analysis

74 The classical measure of the correlation between two time series with a time shift between them  
 75 is given by a cross-correlation function. Its Fourier transform, the cross power spectral density,  
 76 gives the frequency range of correlation. This analysis is best suited for stationary signals with good  
 77 signal-to-noise ratio, otherwise the maximum of the cross-correlation function is not pronounced  
 78 enough to identify a correlation between the time series (Figure 3 a, b).

79 To find the correlation of intermittent and noisy signals, we propose a technique based on  
 80 wavelet analysis and cross correlation analysis which allows to detect both the time scale with  
 81 maximal signal correlation and a possible time-shift. The idea is to use the time-frequency rep-  
 82 resentation offered by the wavelet analysis; and to use as an advantage a compact support of the  
 83 wavelet basis in order to focus the cross-correlation analysis on the significant time scales of the  
 84 signal.

#### 85 3.1. Wavelet transform. Time-frequency representation.

86 The complex wavelet transforms the signal  $x(t)$  using the dilated and time shifted versions of  
 87 a basis function called basis wavelet  $\psi$  Mallat (1999):

$$88 \quad W(a, b) = a^{-1/2} \int_{-\infty}^{\infty} x(t) \psi^* \left( \frac{t-b}{a} \right) dt \quad (1)$$

89 where the wavelet coefficients  $W(a,b)$  give the transformed signal as a function of the translation  
 90 parameter  $b$ , and the dilatation parameter  $a$  (scale). We used the Morlet wavelet which is a complex  
 91 sinus wave with a Gaussian envelope  
 92

$$93 \quad \psi(t) = \pi^{-1/4} e^{i\omega_0 t} e^{-t^2/2}. \quad (2)$$

94

95 We used logarithmically equidistant values for  $a$  (dyadic grid). In this notation, the time is unit-  
 96 less. This wavelet was used to plot the time-frequency wavelet spectrum – the scalogram given by  
 97  $|W(a, b)|^2$ . The Fourier transform of the Morlet wavelet is a Gaussian with positive frequencies  
 98 for  $\omega_0 \geq 5$  (we used  $\omega_0 = 5$ ): The scale - frequency relationship of the Morlet wavelet is given by

$$99 \qquad \qquad \qquad \omega = \frac{\omega_0}{a} \qquad \qquad \qquad (3)$$

101 The wavelet coefficients at every scale are the Hilbert transformed original data (analytic signal)  
 102 bandpass filtered by the Gaussian envelope with center frequency  $\omega$  given by equation 3.

103 *3.2. Linear cross-correlation function of the wavelet coefficients*

104 The next step is the calculation of the linear cross-correlation function  $P(X, Y)$  where the data  
 105  $X$  and  $Y$  are replaced by their complex wavelet coefficients  $Wx = W_x(a, b)$  and  $Wy = W_y(a, b)$

$$106 \qquad P_{Wxy}(a, b) = \frac{\sum_i^{N-b} (Wx_{i+b} - \overline{Wx}) (Wy_i - \overline{Wy})}{\sqrt{\left(\sum_i^N (Wx_i - \overline{Wx})^2\right)} \sqrt{\left(\sum_i^N (Wy_i - \overline{Wy})^2\right)}} \qquad (4)$$

107  
 108 for each scale  $a$  and for reasonable time shifts  $b$ . The cross-correlation function of the wavelet  
 109 coefficients  $P_{W_x, W_y}(a, b)$  is then plotted as a function of scale  $a$  and time delay  $b$  between both  
 110 time series. If the value of  $P_{W_x, W_y}(a, b)$  is close to unity at a scale  $a_d$  and at a time shift  $b_d$ ,  
 111 there is a correlation between signals with dominant frequency corresponding to the scale  $a_d$  and  
 112 a time delay  $b_d$ . Figure 3 shows an example of synthetic time series containing intermittent signals  
 113 superimposed with random noise. The cross-correlation plot of wavelet coefficients in Figure 3 c  
 114 possesses a clear maximum. Its ordinate indicates the scales at which the data contain correlated  
 115 signals, and its abscissa indicates the time shift between them.

116 **4. Data basis and Observations**

117 Figure 4 shows gas temperature data, self-potential and ground temperature data after the end  
 118 of the rain season and re-installation of the sensor in April and till June 2001. Ground temperatures  
 119  $T_4$  and  $T_6$  are not presented here. Sensor  $T_4$  was placed in a permeable erosive channel with much  
 120 higher temperatures (up to 100° C) and larger temporal variations than the other temperature  
 121 sensors, and sensor  $T_6$  was damaged all through the period of observation.

122        Though no rain data in this time interval are available, we suggest that no rainfall happened  
123 between Julian days 110 and 137 (from April 19th to May 16th). As detailed by Friedel et al. (2004),  
124 both self-potential and electrode temperature difference data at this station respond similarly to  
125 the rainfall with typical high amplitudes (up to 300° C in gas temperature and 50 mV in self-  
126 potential data), sharp onset and exponential decay; moreover, a high linear correlation between  
127 the self-potential and electrode temperatures is usually observed during the rainfall. The absence  
128 of such correlated self-potential and electrode temperature signals, as well as the small amplitudes  
129 of variations in all observables suggest that no rainfall happened in this time interval, which was  
130 therefore chosen for a closer study. Amplitude spectra of the time series presented in Figure 4  
131 can be seen in Figure 5. Daily and semi-diurnal variations dominate the ground temperature and  
132 self-potential spectra but are less spectacular in the spectrum of gas temperature where a large part  
133 of the signal energy is distributed between 2 and 8 hour periods. Interestingly, the self potential  
134 spectra also contain some signal energy at these periods, in contrast to ground temperature data.

135        To explore the correlation between self-potential and gas temperature, cross-correlation plots  
136 of wavelet coefficients were calculated as described in section 3; they are shown in Figure 6 a, b and  
137 c. The scale range of correlation between 1 and 8 hours corresponds roughly to the typical signal  
138 durations observed by Zimmer and Erzinger (2003) in gas concentration and gas temperature data.  
139 These periods are hardly visible in the Fourier spectra of the gas temperature in Figure 5 a. The  
140 broad maximum of the correlation is located at scales 1.5-8 hours and a time shift of 130 min at  
141 all three dipoles; self-potential signals precede gas temperature variations. Interestingly, contrary  
142 to the rain season (see discussion in Friedel et al., 2004), no correlation at all is found between  
143 gas temperature and ground temperature (d,e), and no correlation is observed between the self-  
144 potential and ground temperature difference (f). The time frequency representation in Figure 7 a,  
145 b shows striking similarity between the variations of gas temperature and self-potential. Wavelet  
146 coefficients at one scale (2.2 hours) are displayed in c. Gas temperature variations (red curve) are  
147 clearly delayed with respect to the self-potential at both dipoles shown with blue and black lines.

148        Figure 8 plots fumarole temperature data versus self-potential  $U_{21}$ . Both gas and self-potential  
149 data were high-pass filtered with 2.9 h corner period. This choice of the corner period allows  
150 to exclude the 6- and 3h harmonics of the barometric pressure variations. Furthermore, gas  
151 temperature data were time shifted with respect to the self-potential in order to align the correlating

152 signals.

## 153 **5. Discussion**

154 We observed a correlation between the cyclic variations in gas temperature and self-potential  
155 which we attribute to the variations of the magma degassing for the following reasons. Firstly,  
156 we can exclude meteorological influence. As discussed by Friedel et al. (2004), rainfall induced  
157 SP signals can be recognized even without reference precipitation data because they have a very  
158 typical shape, extremely large amplitudes and correlate positively with the ground temperature  
159 data (with the linear correlation coefficient up to  $R^2 = 9.8$  !). Quasi-periodic signals observed in  
160 self-potential and gas temperature data can not be attributed to atmospheric pressure neither, as  
161 typical signal durations vary from 1 to 8 hours and do not generally coincide with the harmonics  
162 of barometric pressure.

163 Secondly, the isotopic studies of Toutain et al. (2009) reveal the magmatic origin of CO<sub>2</sub> in  
164 fumarole Woro. Clear correlation gas concentrations and temperature analyzed by Zimmer and  
165 Erzinger (2003) and presented in Figure 2 suggest that these regularly oscillations of gas parameters  
166 are directly related to magma degassing and are generated by regular oscillations of pressure, which  
167 generate also the related self-potential variations. The whole area is characterized by intense  
168 diffuse degassing, with carbon dioxide concentrations as high as 500 000 ppm in September 2002,  
169 as reported by Toutain et al. (2009). Nevertheless, the ground temperatures at the electrode  
170 locations did not record any temperature changes, related to variations in gas temperature. These  
171 observations indicate that self-potential oscillations are generated by a mechanism other than  
172 diffuse soil degassing or pure temperature effects at the electrode locations. In addition, oscillations  
173 in gas temperature are preceded by self-potential signals with a time shift of more than two hours  
174 indicating a relatively deep source of self-potential. Interestingly, these common oscillations of  
175 self-potential and gas temperature have signatures very different from earlier observations related  
176 to the rain season preceding the eruption in February 2001 (Byrdina et al., 2003; Richter et al.,  
177 2004). These authors observed that ultra-long period (ULP) seismic events were systematically  
178 accompanied by variations of both fumarole temperature (Richter et al., 2004) and self-potential  
179 (Byrdina et al., 2003) without any significant time shift between them. Returning to oscillations  
180 of self-potential and gas temperature during the dry season, we suppose them to be generated



181 by a deeper source than the source of ULP seismicity because of a larger time shift between the  
 182 self-potential and gas temperature. In this case, the time shift between gas temperature and self-  
 183 potential might contain information about the properties of the magmatic conduits or about the  
 184 depth where the pressure pulses are originated.

185 For example, Cigolini et al. (2007) report radon emissions at Stromboli volcano related to  
 186 Palermo earthquake of September 6th, 2002. The regional seismicity was found to be correlated  
 187 with radon emissions and the rate of erupted magma volume. The time delay of radon emissions  
 188 with respect to seismicity was interpreted by viscoelastic properties of the magma chamber. Fur-  
 189 thermore, Olmos et al. (2007) observed a time delay of SO<sub>2</sub> emissions with respect to real time  
 190 seismic amplitude measurements at Santa Ana volcano.

191 Physical models related to cyclic behavior of volcanic degassing in andesitic magmas are usually  
 192 based on nonlinearities caused by the variable viscosity of magma. In these models, viscosity  
 193 of magma depends on volatile content, temperature or pressure, and strongly decreases as the  
 194 degassing rate increases (e.g. Melnik and Sparks, 1999; Lensky et al., 2008). An example is the  
 195 stick-slip model of supersaturated magma degassing developed by Lensky et al. (2008). The gas  
 196 diffuses into the magma, which cannot expand because of the presence of a sticking plug resulting  
 197 in a build-up of pressure. When the pressure exceeds some critical value, the strength of the  
 198 plug, the stick-slip motion occurs and the pressure is relieved. The magma sticks again when the  
 199 pressure falls below the value of dynamic friction. Although the available data are not sufficient  
 200 to attempt a numerical modeling, we can try to understand the information contained in the time  
 201 shift between the gas temperature and the electric signals. In the logic of the stick-slip model we  
 202 expect the electric potential to be generated during the phase where the pressure drop is maximal.  
 203 The time shift would give the travel time of the gas from the source of pressure (e.g. the base of the  
 204 plug) to the surface which would bring some constraints on the depth of the source of pressure as  
 205 we will show in the following. The flow of a compressible ideal gas ( $Pu = \text{constant}$ ) in the porous  
 206 conduit is described by a modification of Darcy equation (e.g. Scheidegger, 1974):

$$207 \quad u = \frac{k}{\mu} \cdot \frac{P_d^2 - P_s^2}{L \cdot P_s} \quad (5)$$

209 where  $u$  is the gas flux velocity in z-direction [m/s],  $k$  is the permeability in [m<sup>-2</sup>],  $\mu$  is the dynamic  
 210 viscosity of the gas in [Pa·s].  $P_d$  and  $P_s$  are the pressures at the source and at the surface in Pa,  
 211 indices stay for "depth" and "surface".  $L$  is the depth of the fumarole origin which can be expressed

212 as  $L = u \cdot \delta t$  where  $\delta t$  is the time delay of the gas in relation with self-potential.

213 Now we estimate the average gas pressure at the pressure source (Figure 9). The relationship  
214 between the gas pressure at magma temperature  $T_d = 1000^\circ\text{C}$  and the gas pressure at the surface,  
215 at the temperature of  $T_s = 450^\circ\text{C}$ , follows from state equation of ideal gas:

$$\left(\frac{P_d}{P_s}\right)^{(\gamma-1)/\gamma} = \frac{T_d}{T_s}, \quad (6)$$

216  
217  
218 where  $\gamma$  is the ratio of specific heats at constant pressure and constant volume  $c_p/c_v \approx 1.3$ . We  
219 obtain from equation (6) the  $P_d = 2\text{ MPa}$  considering the atmospheric pressure at the surface.

220 Returning now to equation (5), we take  $k = 10^{-11}\text{ m}^2$  for the unknown conduit permeability  
221 and  $\mu = 2 \cdot 10^{-5}\text{ Pa}\cdot\text{s}$  for the dynamic viscosity of the water vapor at  $400^\circ\text{C}$  (e.g. Mende and  
222 Simon, 1969), and obtain finally the estimation of darcy velocity  $u \approx 0.04\text{ m/s}$  and the depth of  
223  $\approx 300\text{ m}$ .

224 It is premature to take uncritically any estimations on the basis of self-potential data from  
225 one single location. The present study gives a direct evidence that the pressure variations in the  
226 magma conduit create measurable self-potential variations. However, in order to obtain quantita-  
227 tive information on the pressure source from self-potential monitoring data, it is advantageous to  
228 know the geometry of the flow system from previous structural self-potential studies (e.g. Aizawa  
229 et al., 2009). In addition, it is necessary to use several monitoring stations in order to characterize  
230 the attenuation of the self-potential transients with distance and to obtain a reliable estimate on  
231 the time delay between the self-potential and gas temperature variations.

## 232 6. Conclusion

233 Gas fumarole data and self-potential data collected at Solfatara Woro show correlating events  
234 at scales 1-8 h with a time shift of approximately 130 min. The correlation was observed at all three  
235 dipoles during a time interval of 40 days. The influence of different meteorological factors on both  
236 data sets could be excluded because 1) temperatures at electrode positions showed no correlation  
237 neither with self-potential nor with gas temperatures, 2) the typical signal durations do not coincide  
238 with the harmonics of atmospheric pressure, 3) the absence of response signals characteristic for  
239 rainfall in both self-potential and gas temperature data suggest that the correlation between self-  
240 potential and gas temperature can not be attributed to the rainfall. 4) geochemical data indicate  
241 the magmatic origin of several fumarolic gas components (Toutain et al., 2009).

242 Therefore, the correlated self-potential and gas temperature signals reflect directly the quasi-  
243 periodic variations in magma degassing. The dominant generation mechanism of electric signals  
244 is probably the electrokinetic and thermoelectric effects of gas flow. With higher spatial density  
245 of self-potential dipoles it could be possible to localize the source of the multi-parameter signals  
246 using the information about the amplitude of the self-potential signals as function of the distance  
247 and time delay between the correlated signals.

## 248 7. Acknowledgments

249 The work was partially supported by DFG Ja 590/6. We thank the personnel at BPPTK,  
250 Jogjakarta. We thank Jean Vandemeulebrouck, Eric Delcher and André Revil for interesting  
251 discussions improving the paper. We thank J.F. Lénat and an anonymous reviewer for their con-  
252 structive contributions to our manuscript. The non-polarizable electrodes were borrowed at the  
253 Geophysical Instrument Pool Potsdam (GIPP) of the German Research Centre for Geosciences  
254 (GeoForschungszentrum Potsdam, GFZ). We used Latex, JabRef, and InkSpace open source soft-  
255 ware.

## 256 References

- 257 Aizawa, K., Ogawa, Y., Ishido, T., 2009. Groundwater flow and hydrothermal systems within volcanic edifices:  
258 Delineation by electric self-potential and magnetotellurics. *J. Geophys. Res.* 114, B01208.
- 259 Byrdina, S., Friedel, S., Wassermann, J., Zloticki, J., 2003. Self-potential variations associated with ultra-long-period  
260 seismic signals at Merapi volcano. *Geophys. Res. Lett.* 30 (22), 2156.
- 261 Byrdina, S., Revil, A., Contraires, S., Pant, S., Gautam, U., Koirala, B., Shrestha, P., Tiwari, D., Sapkota, S.,  
262 Perrier, F., 2009. Dipolar self-potential anomaly associated with carbon dioxide and radon flux at Syabru-Bensi  
263 hot springs in central Nepal. *J. Geophys. Res.* 114, B10101.
- 264 Camus, G., Gourgaud, A., Mossand-Berthommier, P., Vincent, P., 2000. Merapi (Central Java, Indonesia) An  
265 outline of the structural and magmatological evolution, with a special emphasis to the major pyroclastic events.  
266 *J. Volcanol. Geoth. Res.* 100 (1-4), 139–163.
- 267 Cigolini, C., Laiolo, M., Coppola, D., 2007. Earthquake-volcano interactions detected from radon degassing at  
268 Stromboli (Italy). *Earth Planet. Sci. Lett.* 257, 511525.
- 269 Crespy, A., Revil, A., Linde, N., Byrdina, S., Jardani, A., Boleve, A., Henry, P., 2008. Detection and localization of  
270 hydromechanical disturbances in a sandbox using the self-potential method. *J. Geophys. Res.* 113, B01205.
- 271 Finizola, A., Lénat, J.-F., Macedo, O., Ramos, D., Thouret, J., Sortino, F., 2004. Fluid circulation and structural  
272 discontinuities inside Misti volcano (Peru) inferred from self-potential measurements. *J. Volcanol. Geoth. Res.* 135,  
273 343–360.

274 Friedel, S., Byrdina, S., Jacobs, F., Zimmer, M., 2004. Self-potential and ground temperature at Merapi volcano  
275 prior to its crisis in the rainy season of 2000-2001. *J. Volcanol. Geoth. Res.* 134 (3), 149 – 168.

276 Harris, A., Ripepe, 2007. Regional earthquake as a trigger for enhanced volcanic activity: Evidence from MODIS  
277 thermal data. *Geophys. Res. Lett.* 34 (2), L02304.

278 Ishido, T., Mizutani, H., 1981. Experimental and theoretical basis of elektrokinetic phenomena in rock-water systems  
279 and its applications to geophysics. *J. Geophys. Res.* 86, 1763–1775.

280 Lénat, J. F., Fitterman, D., Jackson, D., Labazuy, P., 2000. Geoelectrical structure of the central zone of Piton de la  
281 Fournaise volcano (La Réunion). *Bull. Volcanol.* 62, 75–89.

282 Lensky, N. G., Sparks, R., Navon, O., Lyakhovsky, V., 2008. Cyclic activity at Soufriere Hills Volcano, Montserrat:  
283 degassing-induced pressurization and stick-slip extrusion. *Geol. Soc. Spec. Pub.* 307, 169–188.

284 Mallat, S., 1999. *A wavelet tour of signal processing*, 2nd Edition. Academic Press.

285 Melnik, O., Sparks, R., 1999. Non-linear dynamics of lava dome extrusion. *Nature* 402, 37–41.

286 Mende, D., Simon, G., 1969. *Physik - Gleichungen und Tabellen*. VEB Fachbuchverlag Leipzig.

287 Nourbehecht, B., 1963. Irreversible thermodynamic effects in inhomogeneous media and their application in certain  
288 geoelectric problems. Ph.D. thesis, M. I. T., Cambridge.

289 Olmos, R., Barrancos, J., Rivera, C., Barahona, F., López, D. L., Henriquez, B., Hernández, A., Benitez, E.,  
290 Hernández, P. A., Pérez, N. M., Galle, B., 2007. Anomalous Emissions of SO<sub>2</sub> During the Recent Eruption of  
291 Santa Ana Volcano, El Salvador, Central America. *Pure Appl. Geophys.* 164, 24892506.

292 Revil, A., Finizola, A., Piscitelli, A., Rizzo, E., Ricci, T., Crespy, A., Angeletti, B., Balasco, M., Barde-Cabusson,  
293 S., Bennati, L., Bolve, A., Byrdina, S., N., N. C., Gangi, F. D., Morin, J., Perrone, A., Rossi, M., Roulleau, E.,  
294 Suski, B., 2008. Inner structure of La Fossa di Vulcano (Vulcano Island, southern Tyrrhenian Sea, Italy) revealed  
295 by high resolution electric resistivity tomography coupled with self-potential, temperature, and soil CO<sub>2</sub> diffuse  
296 degassing measurements. *J. Geophys. Res.* 113, B07207.

297 Revil, A., Pezard, P. A., Glover, P. W. J., 1999. Streaming potential in porous media 1. Theory of the zeta potential.  
298 *J. Geophys. Res.* 104, 20021–20031.

299 Revil, A., Saracco, G., Labazuy, P., 2003. The volcano-electric effect. *J. Geophys. Res.* 108 (B5), 2251.

300 Richter, G., Wassermann, J., Zimmer, M., , Ohrnberger, M., 2004. Correlation of seismic activity and fumarole  
301 temperature at the Mt. Merapi volcano (Indonesia) in 2000. *J. Volcanol. Geoth. Res.* 135, 331–342.

302 Scheidegger, A. E., 1974. *The physics of flow through porous media*, 3rd Edition. University of Toronto. Press,  
303 Toronto.

304 Surono, S., Jousset, P., Pallister, J., Boichu, M., Buongiorno, M. F., Budisantoso, A., Costa, F., Andreastuti, S.,  
305 Prata, F., Schneider, D., Clarisse, L., Humaida, H., Sumarti, S., Bignami, C., Griswold, J., Carn, S., Oppenheimer,  
306 C., 2011. The 2010 explosive eruption of Java’s Merapi volcano a ”100-year” event. submitted to *J. Volcanol.*  
307 *Geotherm. Res.*

308 Toutain, J., Sortino, F., Baubron, J., Richon, P., Surono, S., Sumatri, S., A.Nonell, 2009. Structure and CO<sub>2</sub> budget  
309 of Merapi volcano during inter-eruptive periods. *Bull. Volcanol.* 71, 815–826.

310 Voight, B., Constantine, E. K., Siswawidjojyo, S., Torley, R., 2000. Historical eruptions of Merapi volcano, Central  
311 Java. *J. Volcanol. Geoth. Res.* 100 (1-4), 69–138.

312 Zimmer, M., Erzinger, J., 2003. Continuous H<sub>2</sub>O, CO<sub>2</sub>, <sup>222</sup>Rn and temperature measurements on Merapi Volcano,  
313 Indonesia. J. Volcanol. Geoth. Res. 125 (1-2), 25 – 38, Understanding volcanoes through multiparameter measure-  
314 ments and their interpretation: In memory of Bruno Martinelli.

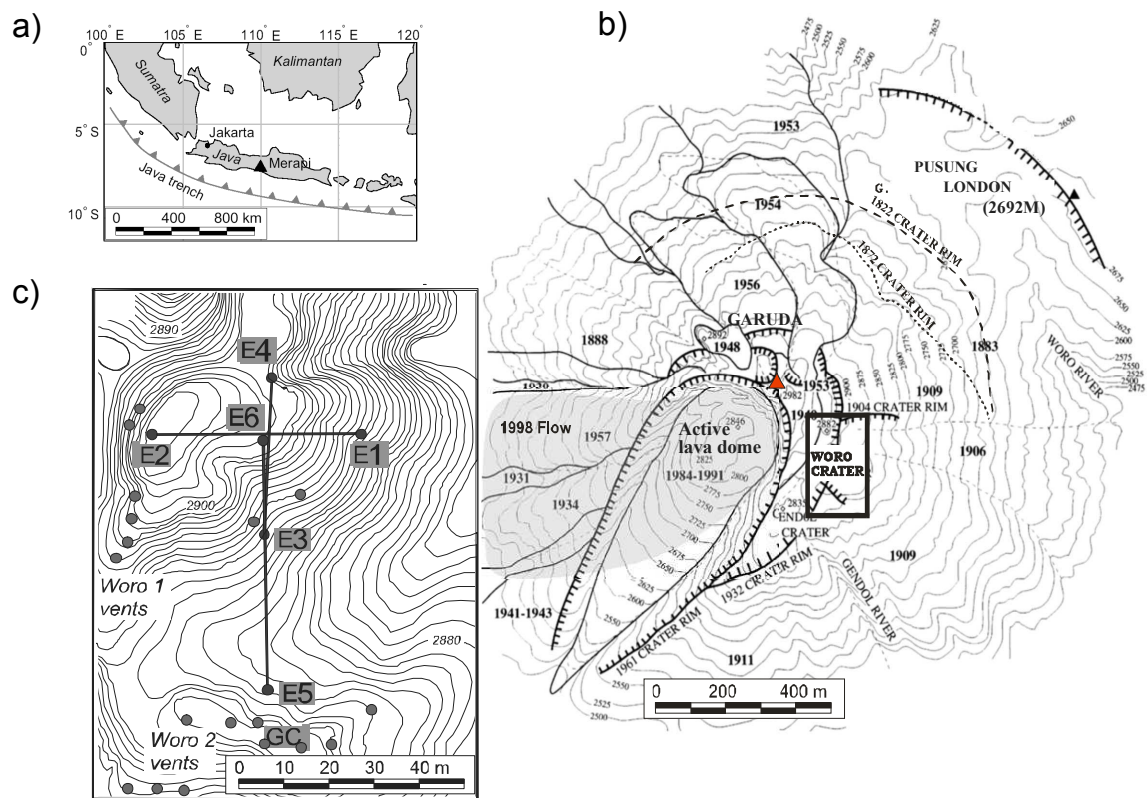


Figure 1: a) Simplified map of Java with location of Merapi volcano and Java trench. b) Summit area of Merapi after Camus et al. (2000), with main lava flows until 2000, crater rims, active dome, and Woro fumarole field. c) Location of our monitoring station at Woro with self-potential dipoles and gas temperature sensor. Gray circles indicate fumaroles (modified from Byrdina et al. (2003)).

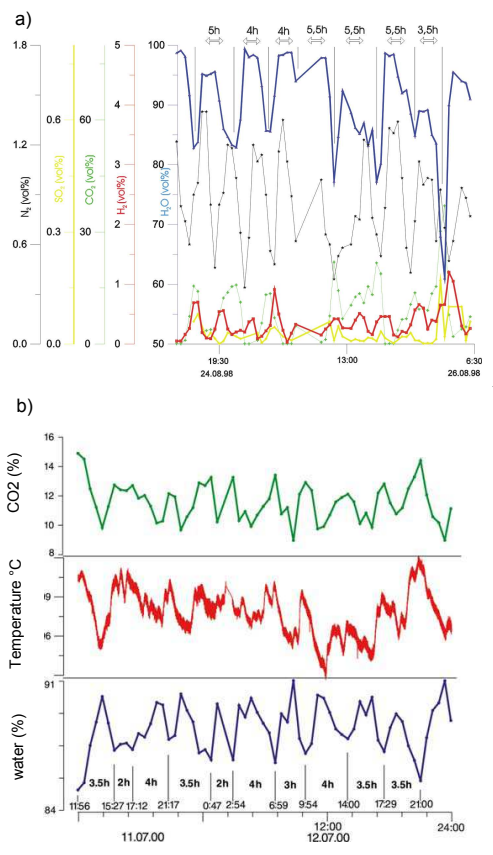


Figure 2: An example of a) gas concentration recorded in 1998 and b) temperature variations recorded in 2000 at Woro solfatara field of Merapi volcano (after Zimmer et al, 2004).

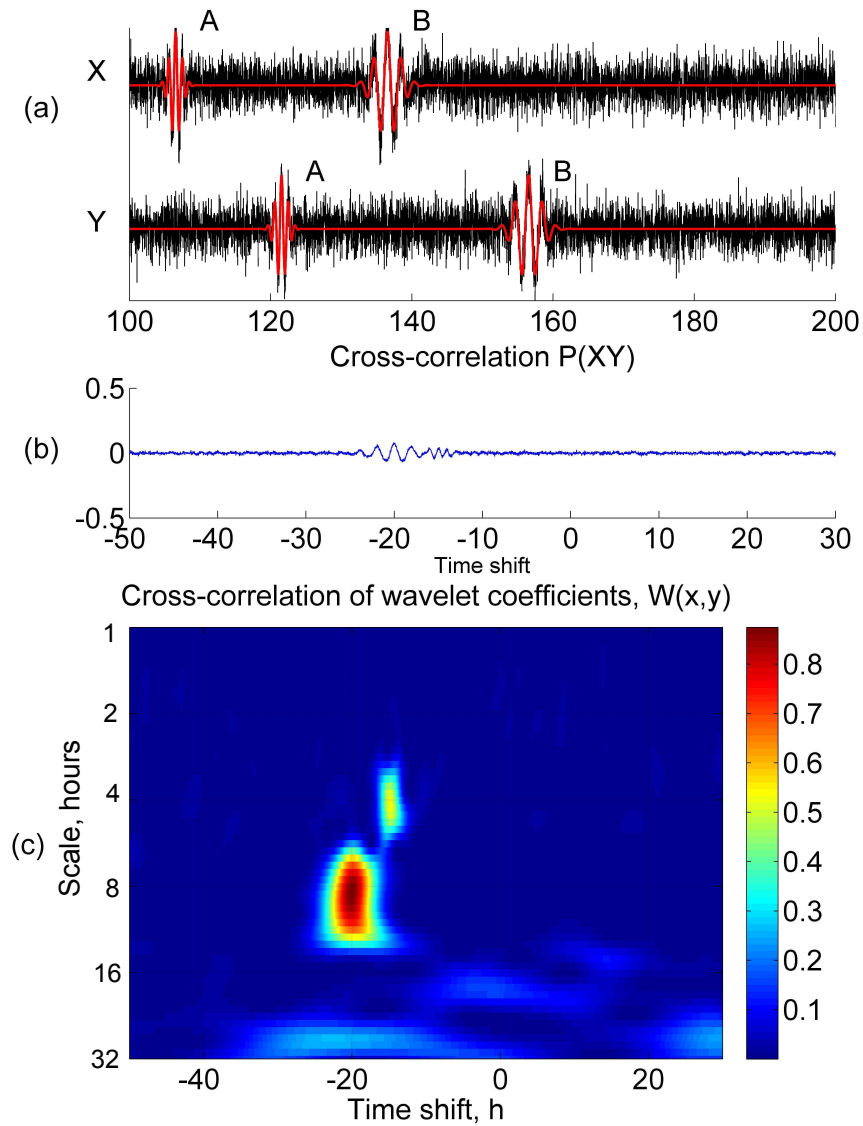


Figure 3: a) Two synthetic data sets  $X$  and  $Y$  (black lines) were created by superimposing random noise with two identical features A and B with time shift 20 and 15 hours. b) Cross-correlation function does not show any clear maxima. c) Cross-correlation of wavelet coefficients of  $X$  and  $Y$  separates the scales of correlation and gives the time shifts between both signals.



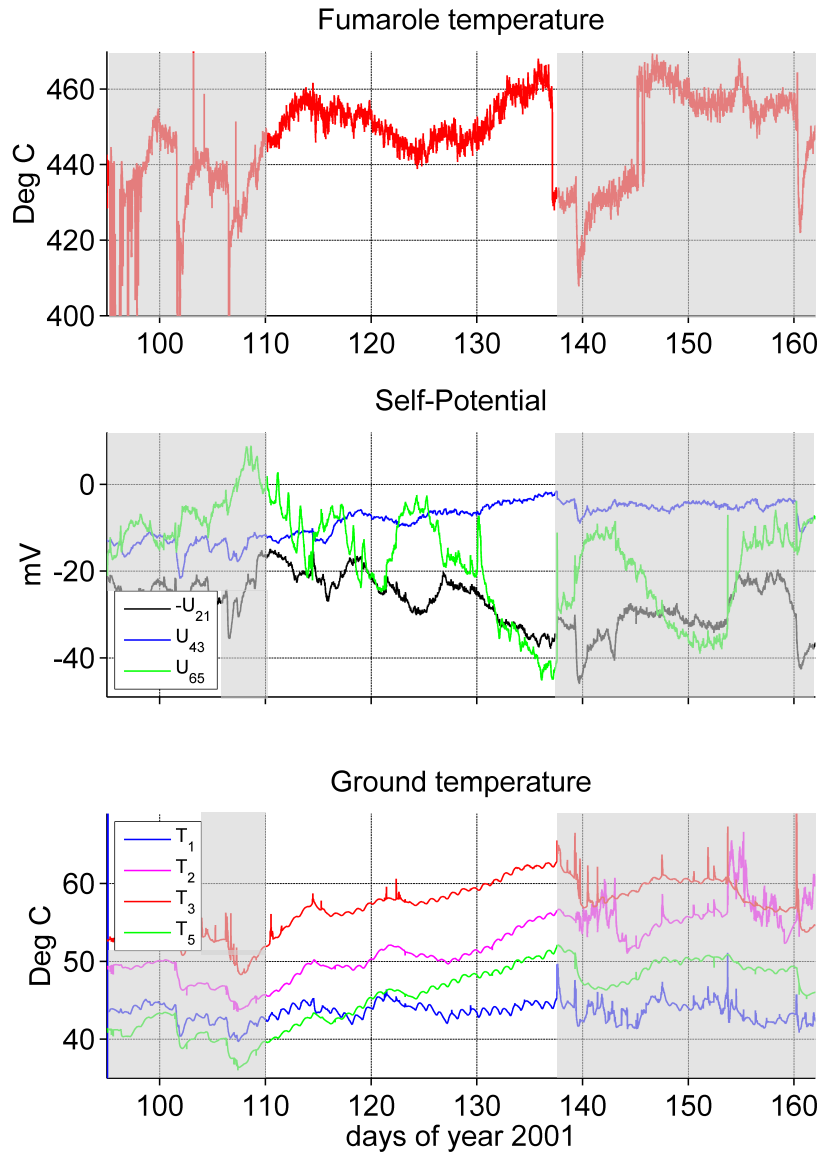


Figure 4: Time series of fumarolic temperature, self-potential and ground temperature. See Figure 1 for location of the sensors. Data from the time period between day 110 and 137 of year 2001 without any perturbations were taken for a further study.

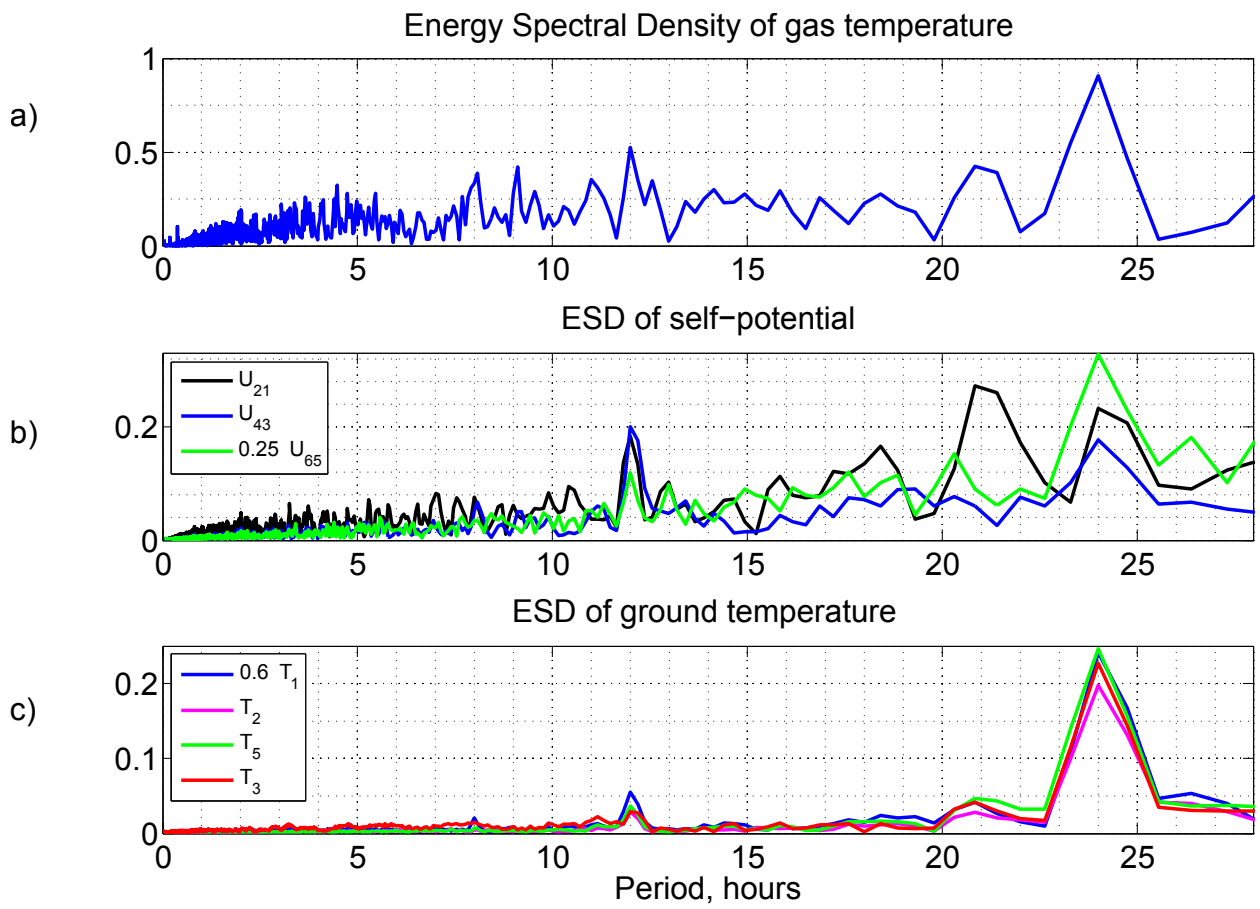


Figure 5: Energy spectral density of the time series presented in Figure 4 in the time period between day 110 and 137 of year 2001.

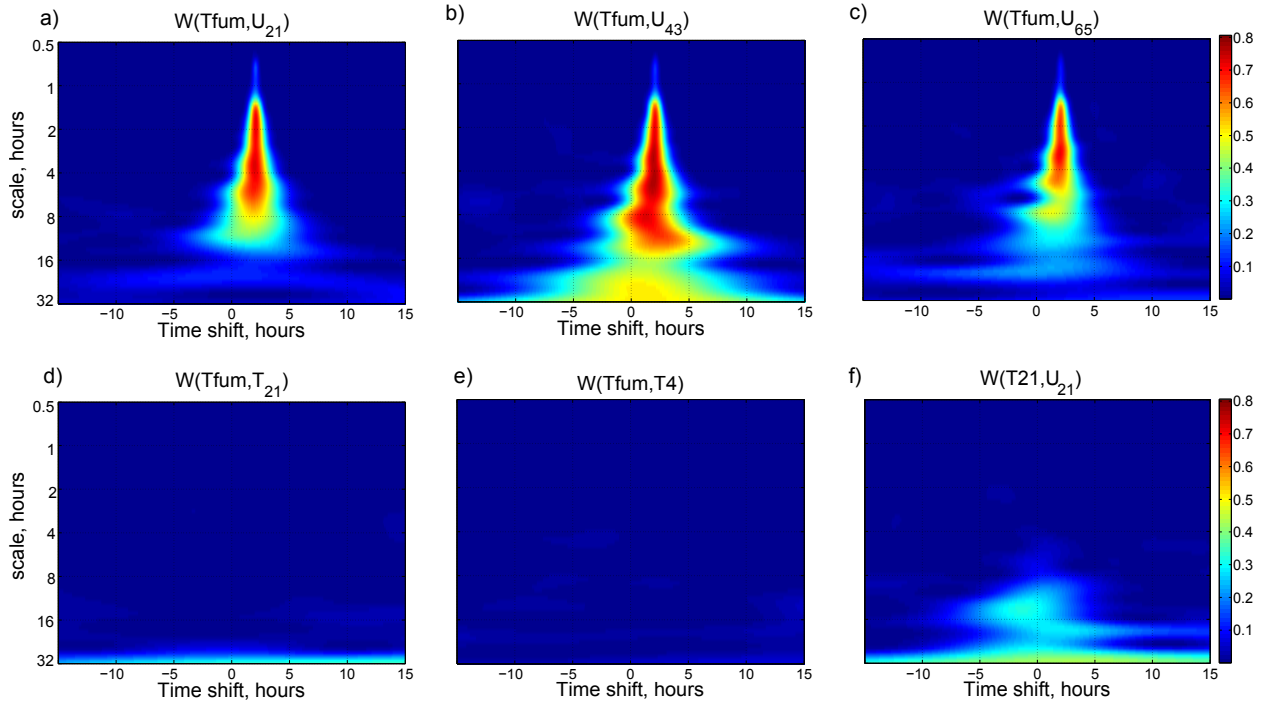


Figure 6: The cross-correlation of wavelet coefficients for a)  $T_{fum}$  and  $U_{21}$ , b)  $T_{fum}$  and  $U_{43}$ , c)  $T_{fum}$  and  $U_{65}$ , d)  $T_{fum}$  and  $T_{21}$ , e)  $T_{fum}$  and  $T_4$ , f)  $T_{21}$  and  $U_{21}$ . High values of  $W(T_{fum}, U)$  are encountered at scales 1-8 hours indicating a correlation between the fumarole gas temperature and SP. A time shift between the correlated signals is approximately 130 minutes, the self-potential variations precede the corresponding variations of fumarole temperature. Interestingly, there is no correlation between the gas and the ground temperature (d, e); there is no correlation between the electrode temperature difference and the self-potential (f).

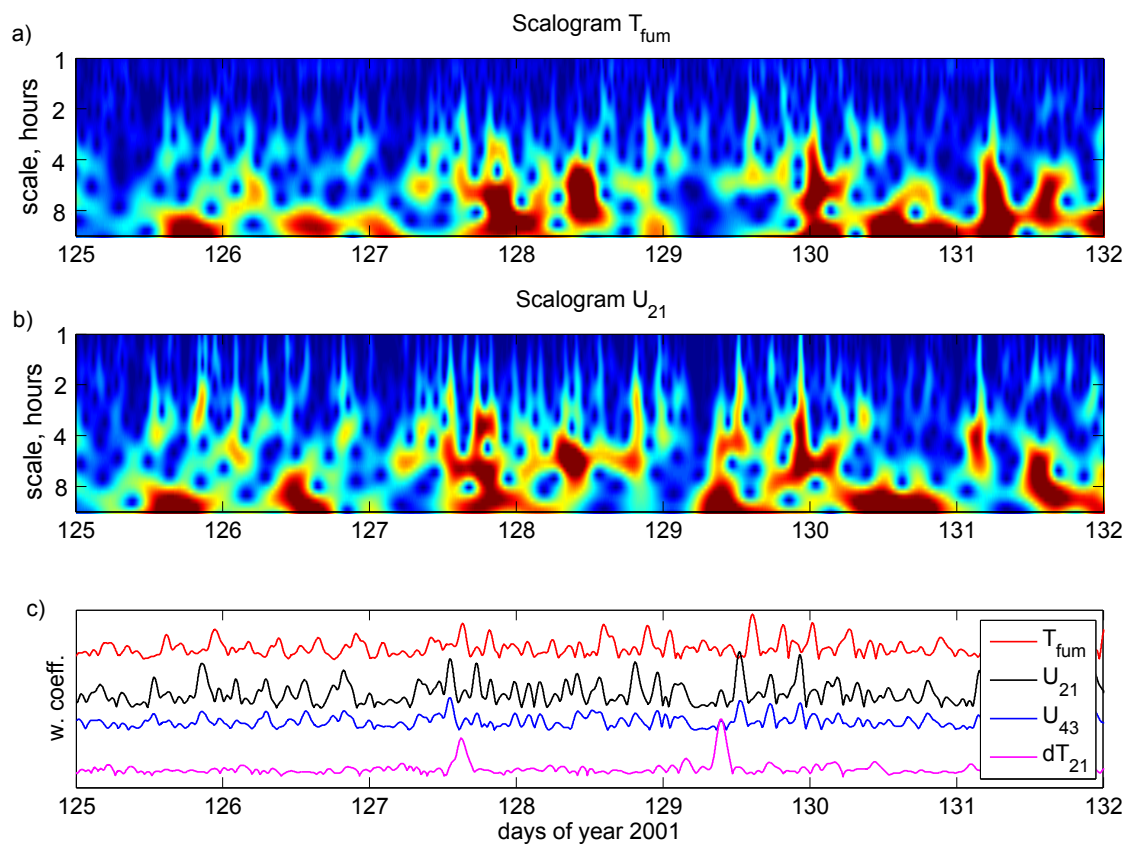


Figure 7: Time-frequency representation of gas temperature (a) and self-potential dipole  $U_{21}$  (b). Time in Julian days is represented in  $X$  and scales in  $Y$  axes. c) Wavelet coefficients at scale of maximal correlation ( $\approx 2.2$  hours) for the gas temperature, self-potential at two dipoles, and for electrode temperature difference  $T_2 - T_1$ .

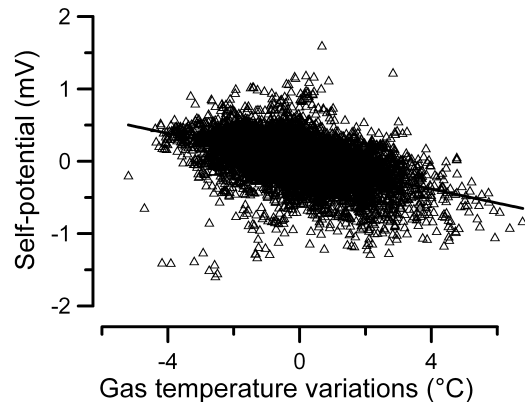


Figure 8: Gas temperature data versus self-potential  $U_{21}$  at period range from 2 min to 170 min. Both kinds of time series were high-pass filtered, gas temperature data were time shifted to align the correlated signals.

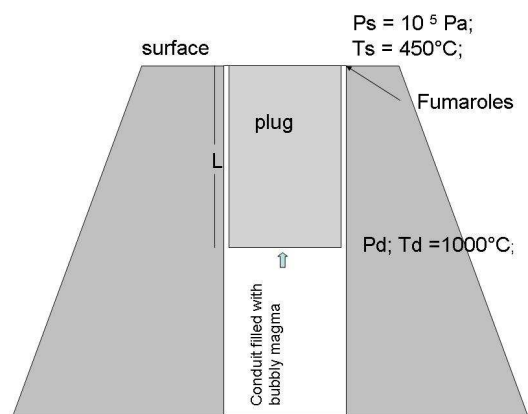


Figure 9: Parameters entering equations 5 and 6 which govern the flow of a compressible fluid in the fumarole conduit (see text).